Tree-ring Science in Hydroclimatology: Some Great Basin Examples

Franco Biondi, University of Nevada, Reno

Franco Biondi is a dendroecologist whose main interests are climate and forest dynamics, ecohydrological changes, and spatial processes. He holds an Italian doctorate in forestry from the Università di Firenze, and MS and PhD degrees in watershed management and geosciences from the University of Arizona in Tucson. He is currently Professor and DendroLab Director at the University of Nevada, Reno, where he is also a member of four interdisciplinary graduate programs: Hydrologic Sciences; Environmental Sciences; Atmospheric Sciences; and Ecology, Evolution, and Conservation Biology. Together with his students and colleagues, he has conducted research projects in North America and Italy on issues related to drought and water resources and funded by the National Science Foundation (including a CAREER award in 2002-2008 and an EAGER award in 2012-2014), the National Oceanic and Atmospheric Administration, the Bureau of Land Management, and the National Geographic Society. With approximately 200 publications and conference presentations, Google Scholar gives him an H-index of 27 and an i10-index of 51. In recent years he has collaborated with the Southern Nevada Water Authority and the Truckee Meadows Water Authority on issues dealing with drought planning and long-term water resource management.

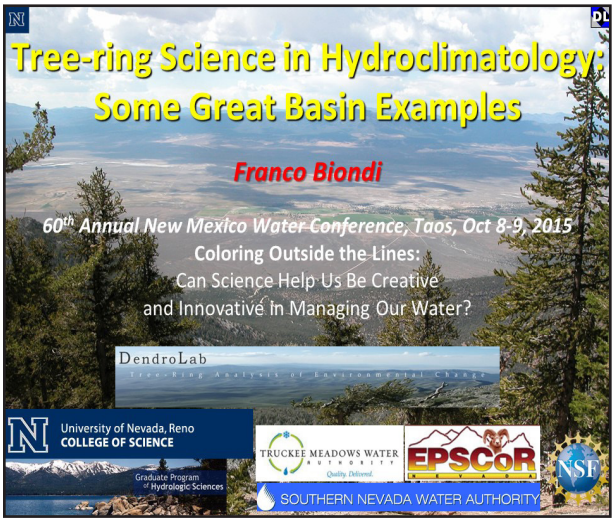

Figure 1. Presentation introduction.

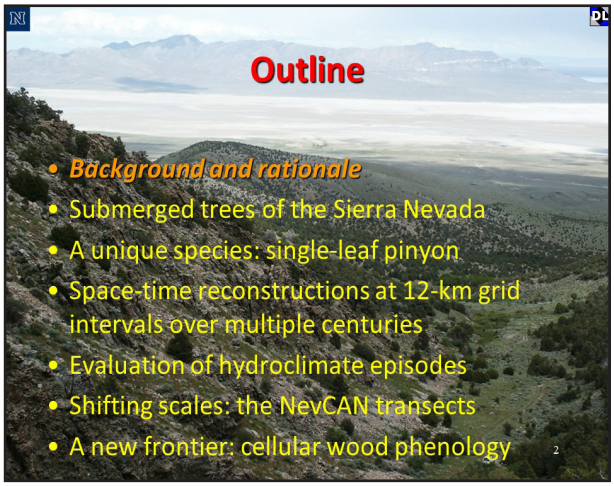

Figure 2. Presentation outline.

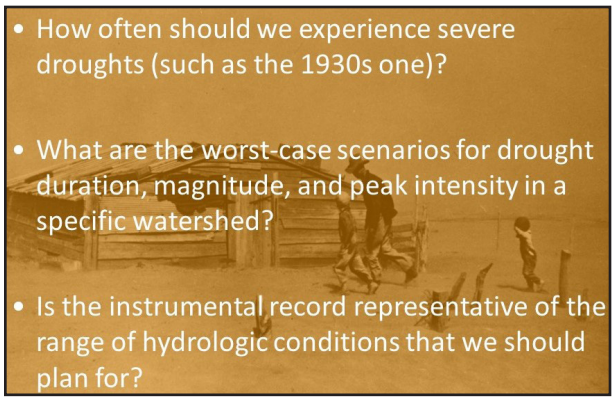

Figure 3. Major hydrological questions.
A typical example from hydrology would be our understanding of the Colorado River flow. The "Compact" that regulates allocation of Colorado River water among western states (and Mexico) was first signed in 1922 using data starting in 1905, a period that has been characterized as unusually wet by comparison with both the instrumental record to date as well as proxy records for the past few centuries.

Figure 4. Recent articles on tree mortality.

Figure 5. Use of wildlife regime practices in forest fire management.

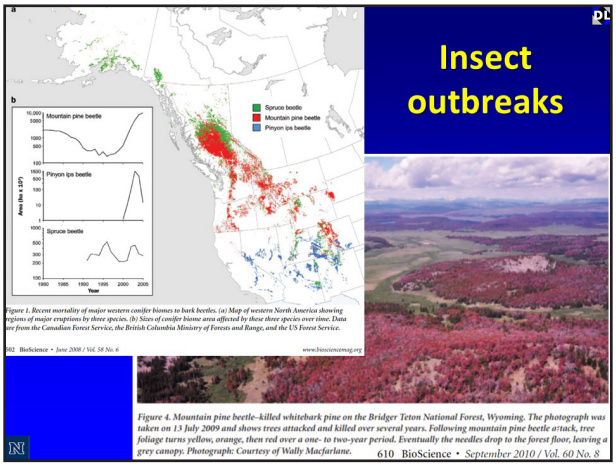

Figure 6. Insect outbreaks.

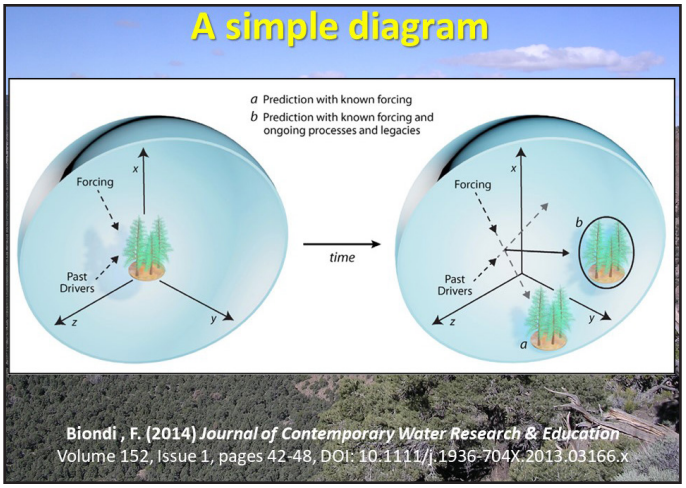

Figure 7. Diagram showing how the trajectory over time of an ecosystem and its features cannot be correctly predicted using only its current conditions and the expected forcing, since the future ecosystem will ultimately be influenced by the effect of past drivers. Consider how important it is in medicine to know the medical history of a patient for a correct diagnosis of present/future disease. Simplicity of expression does not imply simplicity of content. Seek the company of those who search for truth; run from those who have found it.

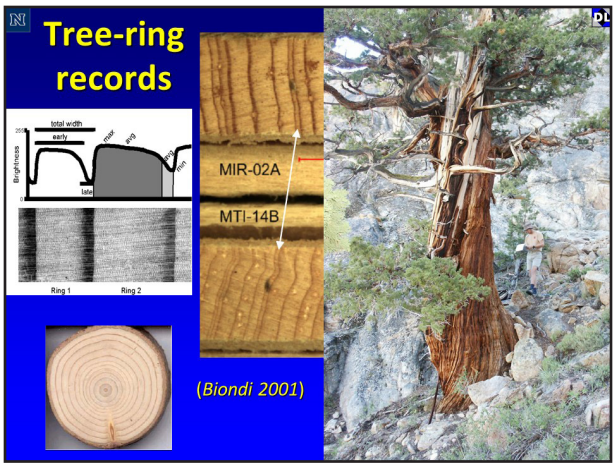

Figure 8. The basic principle of dendrochronology. Crossdating requires more than just a few rings. Wood accumulation usually proceeds from the crown downward, so that in particularly difficult years, the cambium may not become active near the base of the tree. The following example can't be used in dendrochronology because it has too few rings, is too large, and most likely from a plantation, park, or garden.

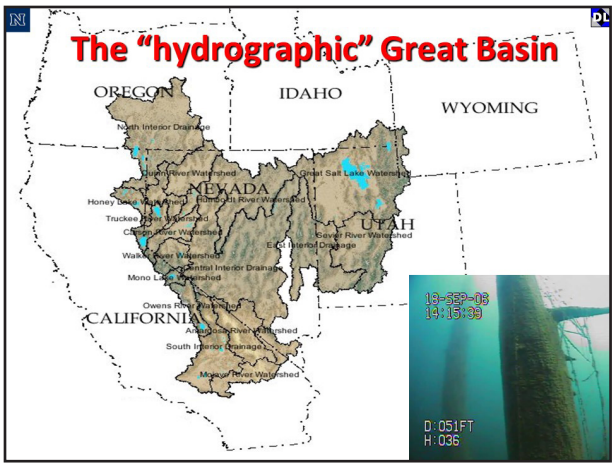

Figure 9. The "hydrographic" Great Basin. The eastern slopes of the Sierra Nevada are actually part of the Great Basin, and this map is being used for this region, based on the hydrographic definition in Grayson's book. Nevada has most of the Great Basin (Basin and Range Province). It spans 7° latitude, from 35 to 42° N, a linear distance of 800 km. Elevation is ~1000 m higher in the north than in the south. The combination of latitude and elevation makes the south much warmer than the north.

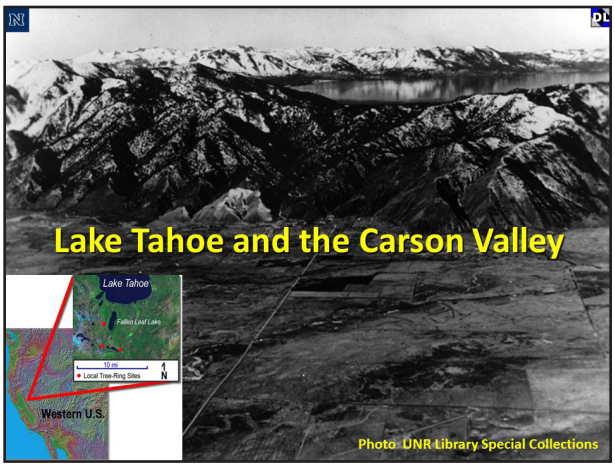

Figure 10. Lake Tahoe and the Carson Valley. Lake Tahoe is a unique feature in North American landscapes. In the early 2000s, Lake Tahoe dropped about 60 cm over two years, thereby getting below its natural rim twice. In the 1930s it reached a minimum of 37 cm below the sill.

Figure 11. Submerged trees from Fallen Leaf Lake.

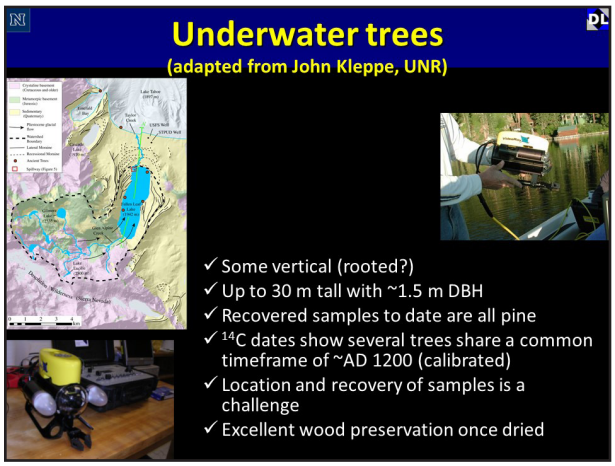

Figure 12. The identification of underwater stumps and trees done by John Kleppe using a remotely operated vehicle. This ROV has been extensively tested in Fallen Leaf Lake, where a total of 13 submerged trees have been located. Some of these trees are over 30 m tall with a circumference greater than four meters (Kleppe 2005). The samples forwarded to the DendroLab for tree-ring analysis all appear to be pine (logdepole or yellow), species that are pervasive in the surrounding mixed-conifer forests. Recovered samples show extensive exterior weathering and perfectly preserved wood underneath.

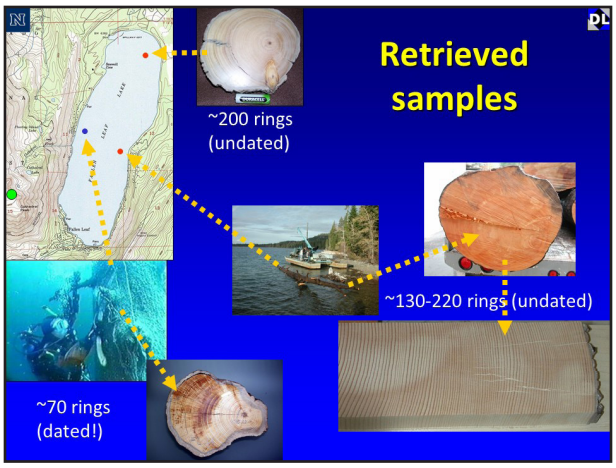

Figure 13. Samples of tree ring dating were collected by cutting branches from trees standing underwater. Two samples contained enough rings to allow the possibility of dendrochronological dating: these branch cross-sections are shown together with their location in the lake. Additional tree-ring samples were obtained by raising a log from the bottom of the lake using a large floating crane. Then a section cut from the log at a height of about 5.2 m above root level was used for tree-ring dating. For dating purposes, the only local species that could yield a chronology longer than 1,000 years was western juniper. Samples were collected from live and dead trees at three sites around Fallen Leaf Lake, and the samples were analyzed using standard dendrochronological methods. Of the three underwater samples, only one could be crossdated with the master chronology. This was the branch cross-section shown before (blue dot in the lake map), which matched the period AD 1085-1134 both visually and numerically.

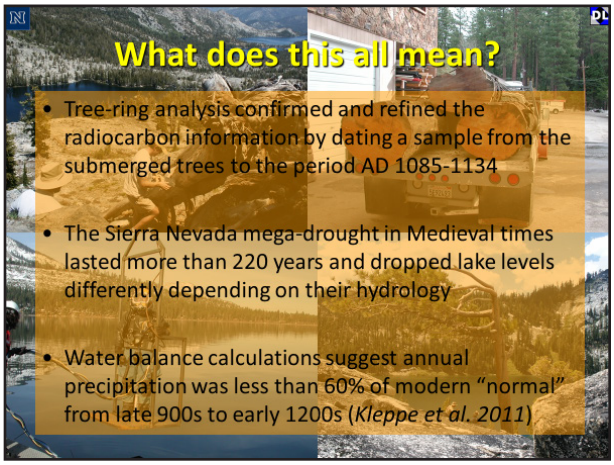

Figure 14. What do the results mean? Such extended drought in the region may have occurred once or twice per millennium. As tree-ring samples are collected, dated, and entered into a master chronology, they will also provide a way to construct a continuous, annually resolved record that could span several millennia, because some of these submerged trees, according to already conducted radiocarbon analysis, date back to the mid-Holocene.

Figure 15. Single-leaf pinyon is a unique species: it is the only one-needle pine in the world! Single-leaf pinyon is found in a large portion of the Great Basin, so it's adapted to extreme drought and severely cold climate. It is a fire-adapted species, with a fire regime that is considered to be a mixture of low- and high-intensity fires. Its arrival in the Great Basin is relatively recent.

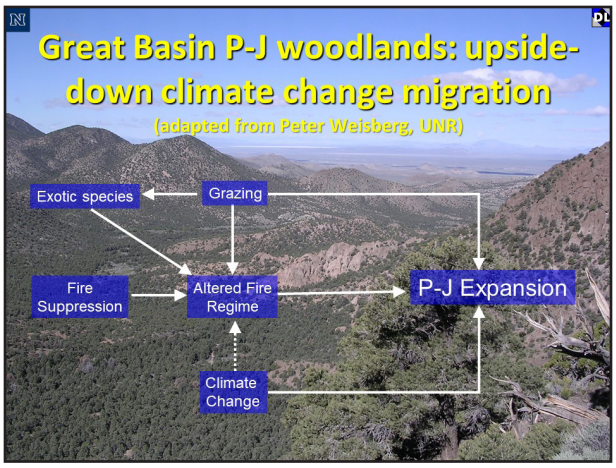

Figure 16. Great Basin P-J woodlands: upside-down climate change migration. There are many examples that show how information on long-term climatic change can help in understanding changes in the environments. For instance, in the Great Basin, pinyon-juniper (P-J) ecosystems are expanding downslope, a trend that's been present since Euro-American settlement, and is opposite to the "upslope migration" that climate change models have predicted. The expansion of pinyon-juniper woodlands illustrates the regional environmental changes managers are confronted with due to rapid urban and population growth. The interaction of landscape-level factors in determining the recent increase of P-J vegetation is not well understood, even though it has important implications for fire management in the Great Basin.

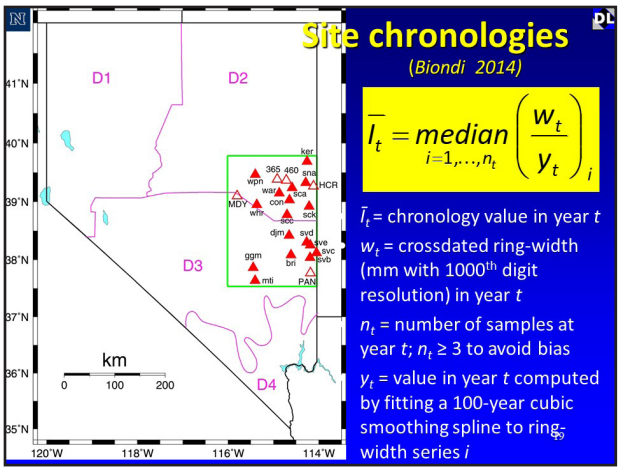

Figure 17. Map of 22 chronologies (all from Pinus monophylla samples) selected since they had a correlation >0.4 with Oct-May precipitation in their PRISM cell. PIMO: red triangles, solid for DendroLab sites and empty for ITRDB sites. The period 1650-1976 was selected to include the 17 DendroLab chronologies and five ITRDB chronologies that effectively improved spatial coverage. The chronology value is a median annual index, and the cubic smoothing spline has a 50% frequency response at a period of 100 years; wt / yt = dimensionless index value of sample i in year t.

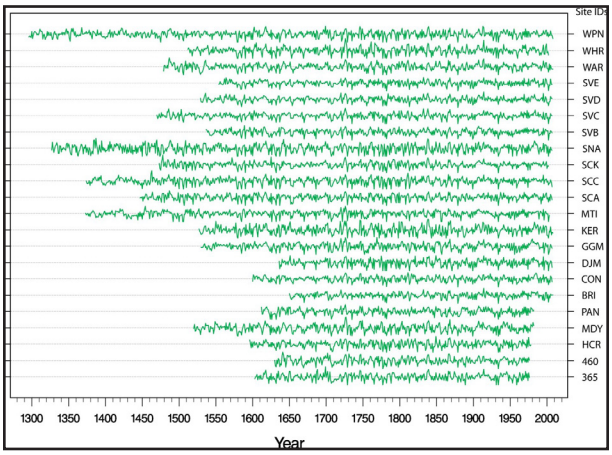

Figure 18. Tree-ring chronologies graphed. With one sample, the longest chronology starts in 958; overall mean segment length exceeds 300 years. The 22 pinyon tree-ring chronologies show remarkable agreement during periods of major droughts, such as the late 1500s one and the Dust Bowl period (1930s).

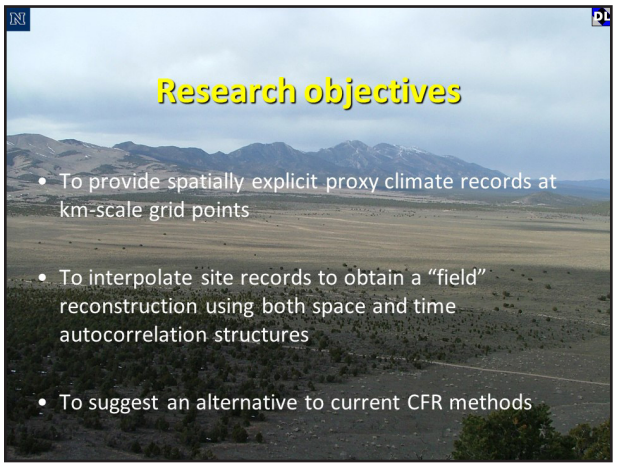

Figure 19. Research objectives.

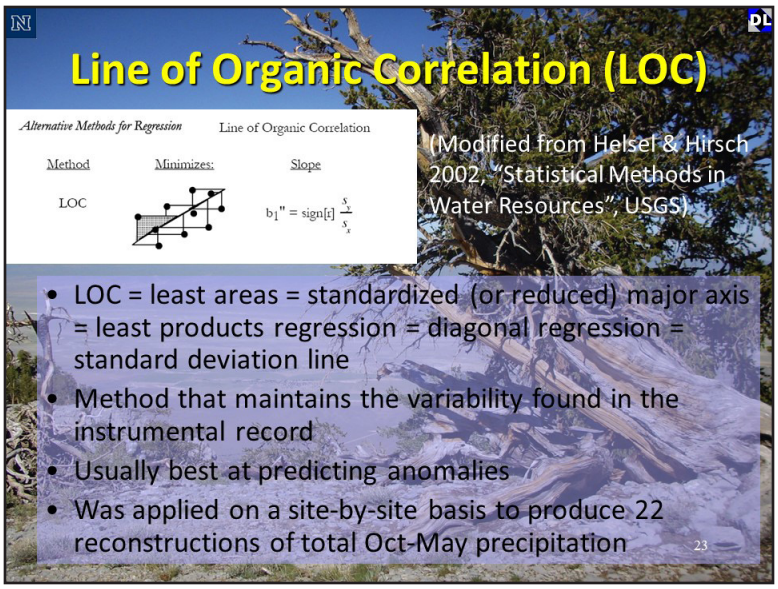

Figure 20. Line of organic correlation (LOC).

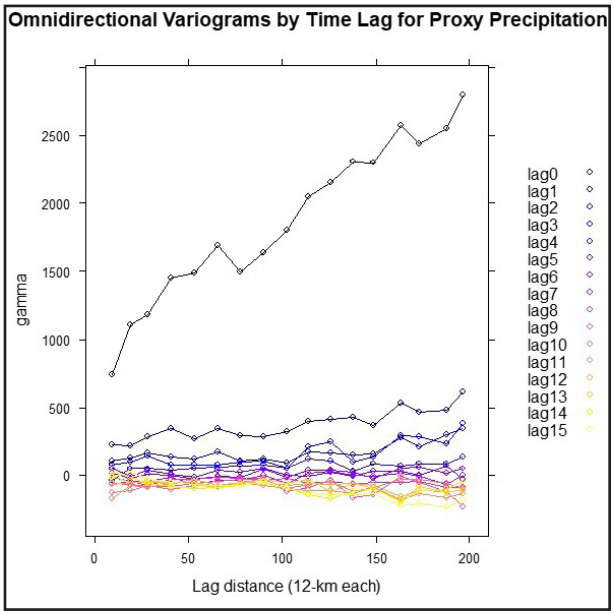

Figure 21. Omnidirectional variograms by time lag for proxy precipitation.

The state-space model

$$Z_t = X_t\beta + KY_t + (\varepsilon_t + \omega_t)$$
$$Y_t = GY_{t-1} + \eta_t$$

The initial state at time $t = 0$ is given by $Y_0 \sim N_p(\mu_0, \Sigma_0)$.

The errors

$$\eta_t \sim N_p(0, \Sigma_\eta)$$
$$(\varepsilon_t + \omega_t) = e_t \sim N_n(0, \Sigma_e)$$

Putting $\sigma_\varepsilon^2 = \gamma\sigma_\omega^2$ we obtain

$$\Sigma_e = \sigma_\omega^2 \begin{cases} 1+\gamma & h = 0 \\ C_\theta(h) & h > 0 \end{cases}$$

Figure 22. The estimator of the spatio-temporal process for a new location (i.e., grid point) at a given time (i.e., year) can be obtained using the EM algorithm.

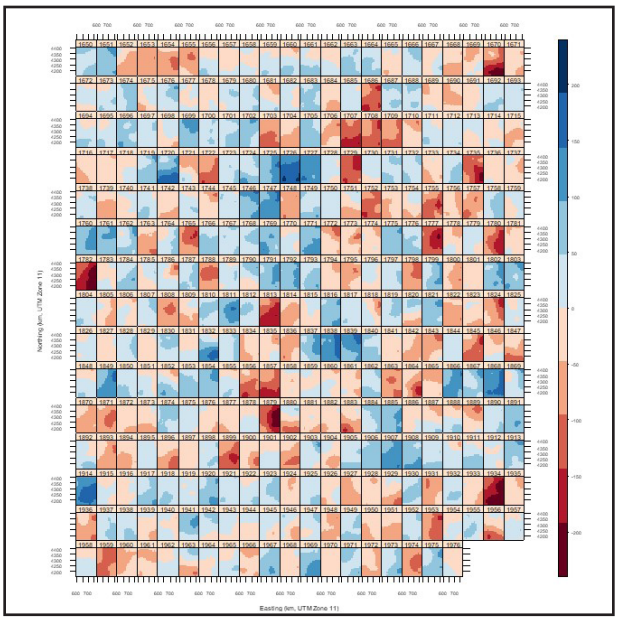

Figure 23. Space-time kriging. Plot obtained with the commands in SNWA_spacetime.R using 11 intervals for the -240 to 240 range of Oct-May precipitation anomalies. This object is plotted using the symbols and scale for the "SpatialPixels" class.

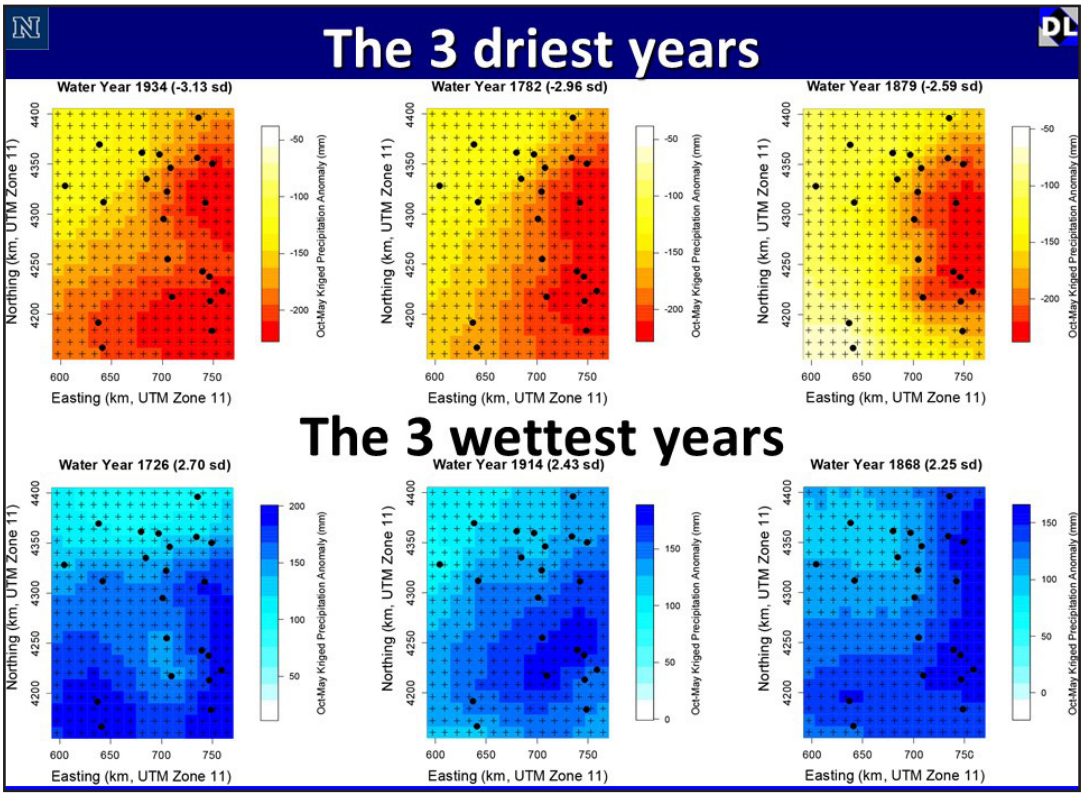

Figure 24. Graphs showing the three wettest and three driest years. Differences in pseudocolor patterns matched those in actual kriged estimates, showing that spatial variability was generally higher in the wet years (north-south, east-west, and centered patterns) than in the dry ones (mostly east-west patterns).

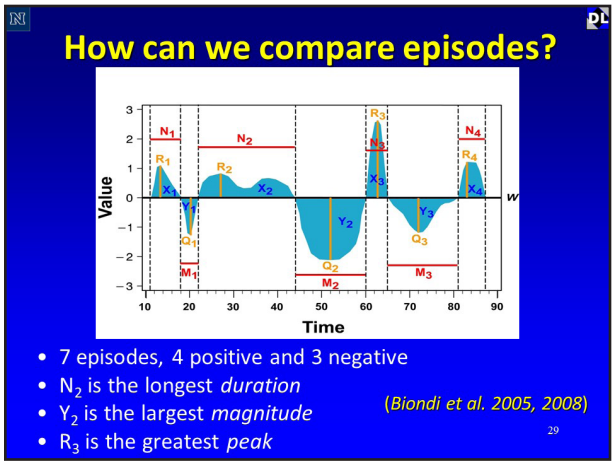

Figure 25. Episode comparison.

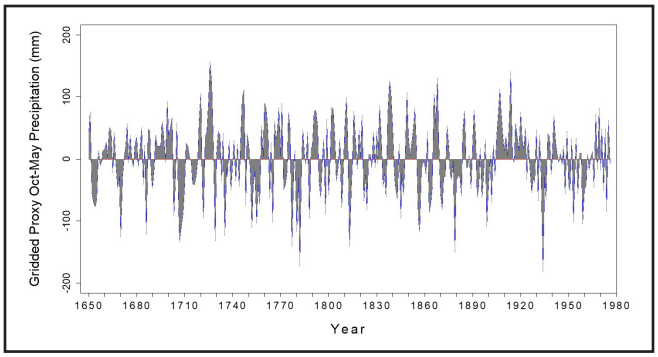

Figure 26. Mean of 315 grid-point proxy precipitation anomalies.

The 10 (out of 150) annual strongest episodes (1650-1976)

Start (year)	End (year)	Episode Type	Duration (years)	Absolute Magnitude (mm)	Absolute Maximum (mm)	Score
1905	1915	Pos	11	588.6	140.447	444
1876	1883	Neg	8	356.9	150.118	440
1723	1728	Pos	6	469.5	156.043	438
1706	1710	Neg	5	422.9	132.172	428
1751	1757	Neg	7	417.7	110.287	427
1848	1855	Pos	8	329.6	106.57	424
1780	1783	Neg	4	326.4	171.252	420
1933	1936	Neg	4	303.2	181.21	418
1837	1840	Pos	4	358.2	125.019	414
1856	1861	Neg	6	266.8	117.025	413

Figure 27. Table showing the ten strongest episodes. The early 1900s pluvial is the strongest episode in the 327-year record, followed by the late 1800s drought.

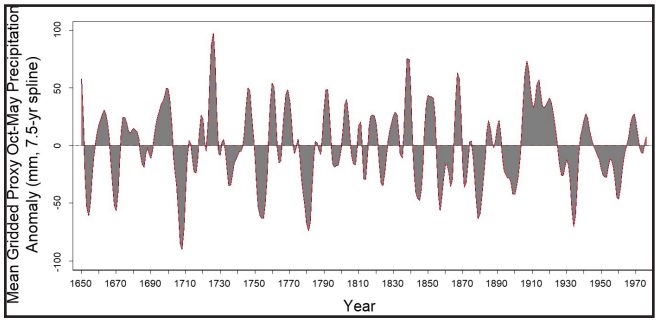

Figure 28. Grid-point reconstructions based on the 7.5-year cubic spline smoothing, showing climate episodes.

The 10 (out of 55) interannual strongest episodes (1650-1976)

Start (year)	End (year)	Episode Type	Duration (years)	Absolute Magnitude (mm)	Absolute Maximum (mm)	Score
1904	1924	Pos	21	836.2	73	161
1925	1937	Neg	13	373.7	70	154
1703	1711	Neg	9	421.8	90	153
1776	1784	Neg	9	382.0	74	150
1946	1964	Neg	19	381.0	46	142
1750	1757	Neg	8	357.1	63	139
1692	1702	Pos	11	354.9	50	137
1855	1864	Neg	10	298.5	56	137
1876	1883	Neg	8	290.7	63	134
1723	1728	Pos	6	358.2	97	133

Figure 29. Table showing the ten interannual strongest episodes. The early 1900s pluvial is still the strongest episode in the 327-year record, but now it is followed by five droughts, of which the 1930s is the strongest one.

Figure 30. NevCAN on the Nevada climate change portal.

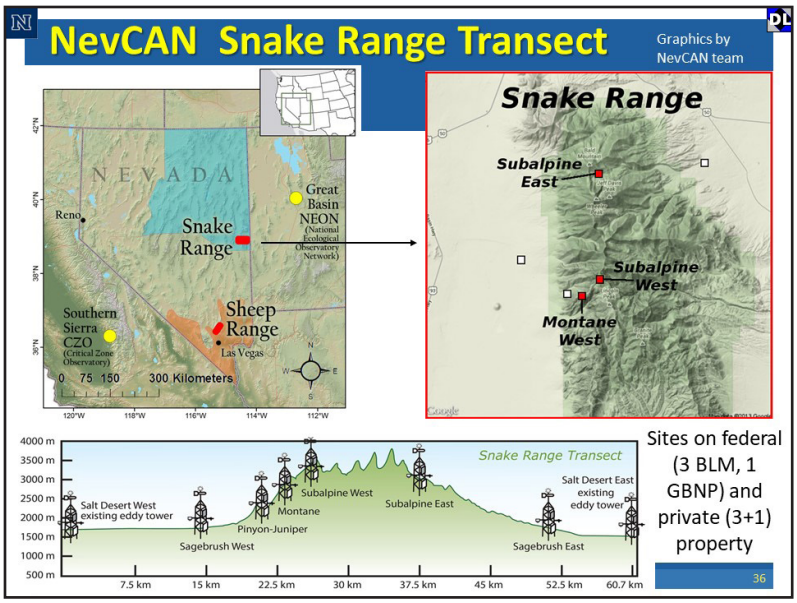

Figure 31. Snake Range transect.

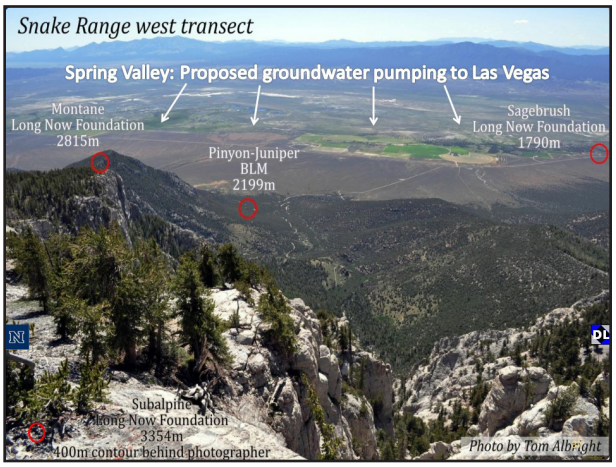

Figure 32. Image showing environmental controls on wood formation.

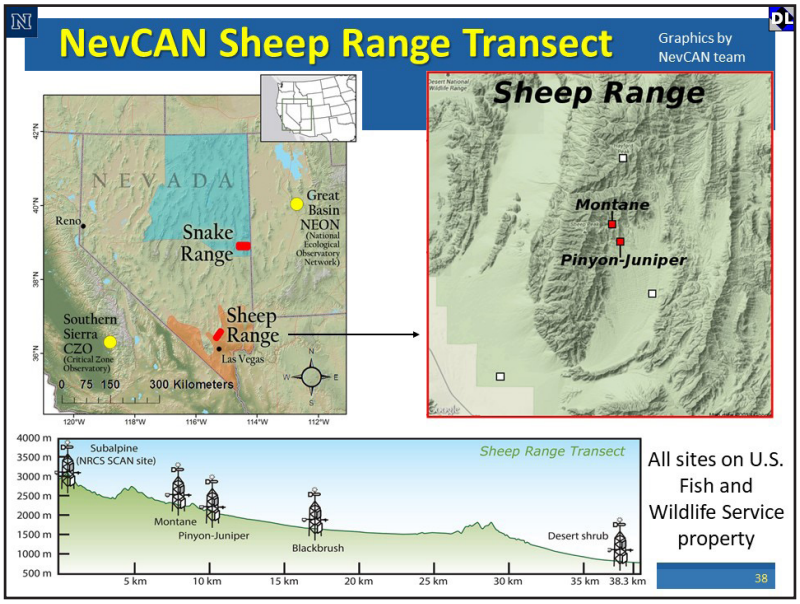

Figure 33. Sheep Range transect. The Sheep Range is located at the boundary of Nevada Climate Division 4 (orange shading), while the Snake Range is at the southern edge of Climate Division 2 (cyan shading). Site locations along each transect are shown using elevation profiles and topographic relief maps; on the latter, sites already sampled for wood anatomy are marked with red squares.

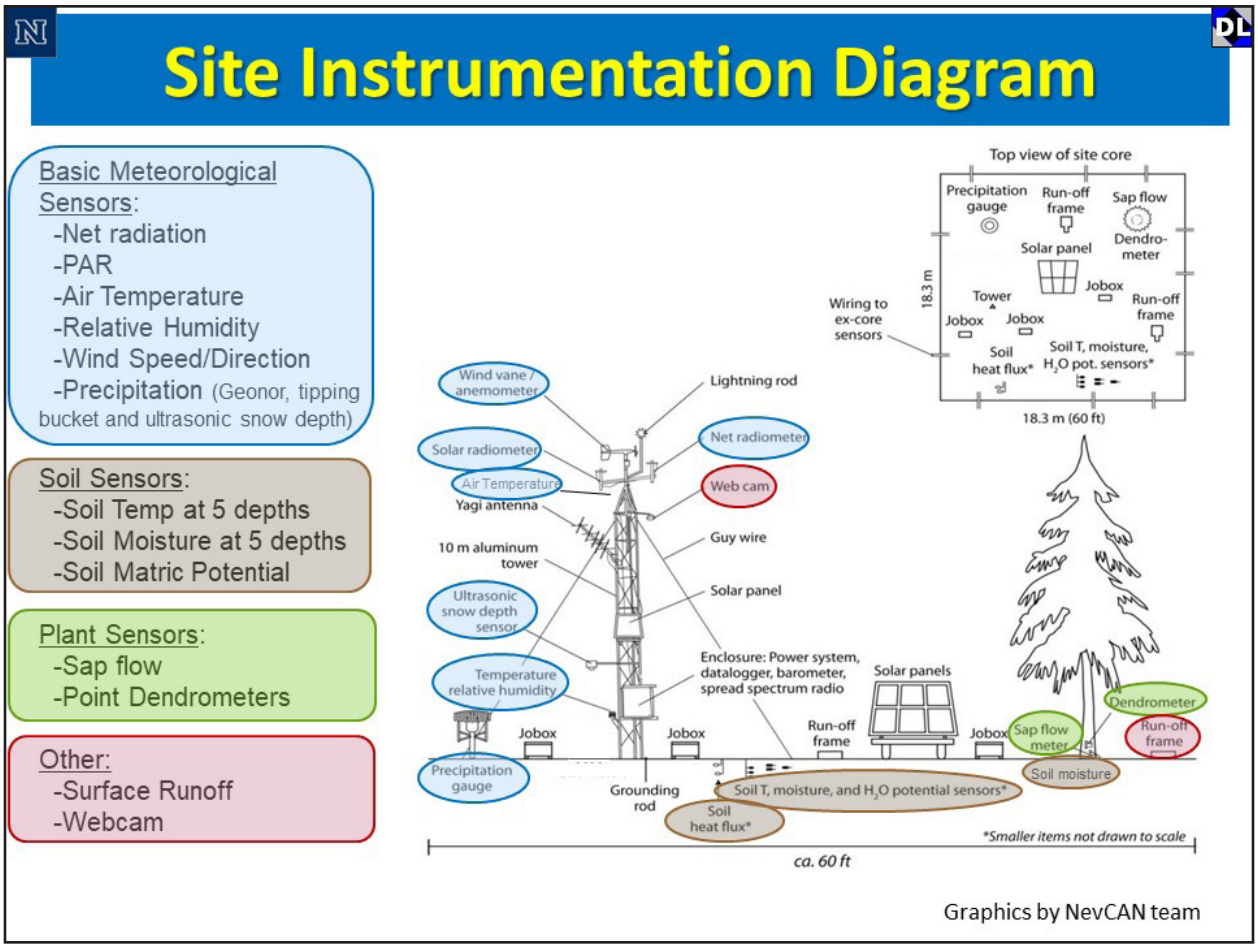

Figure 34. Site instrumentation design.

Figure 35. Research needs observations (RENO)

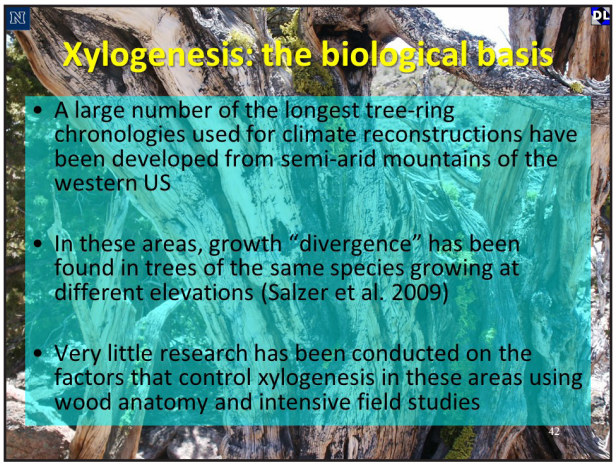

Figure 36. The biological basis of Xylogenesis in trees.

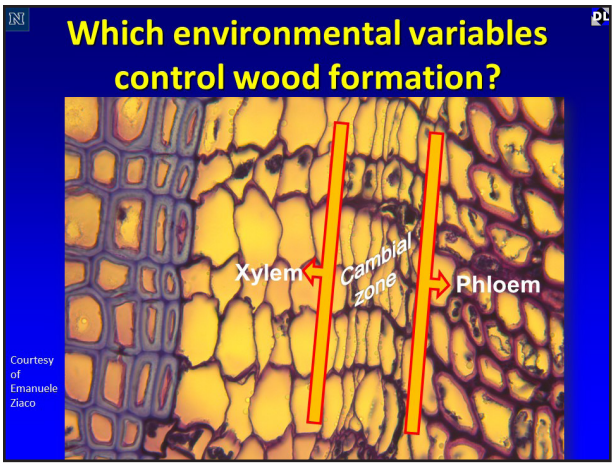

Figure 37. The process of wood formation and tree growth. During xylogenesis, the processes of cell production, radial enlargement, and wall thickening are separated in time and space resulting in a radial pattern of discrete developmental zones. Together these processes determine the final morphology of the xylem and the overall radial growth increment of the tree. Using microsections and repeated sampling during the year, we plan to obtain a more mechanistic understanding of tree growth.

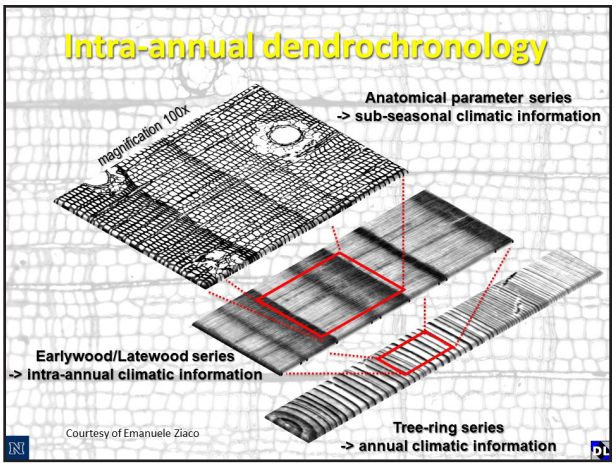

Figure 38. Intra-annual dendrochronology.

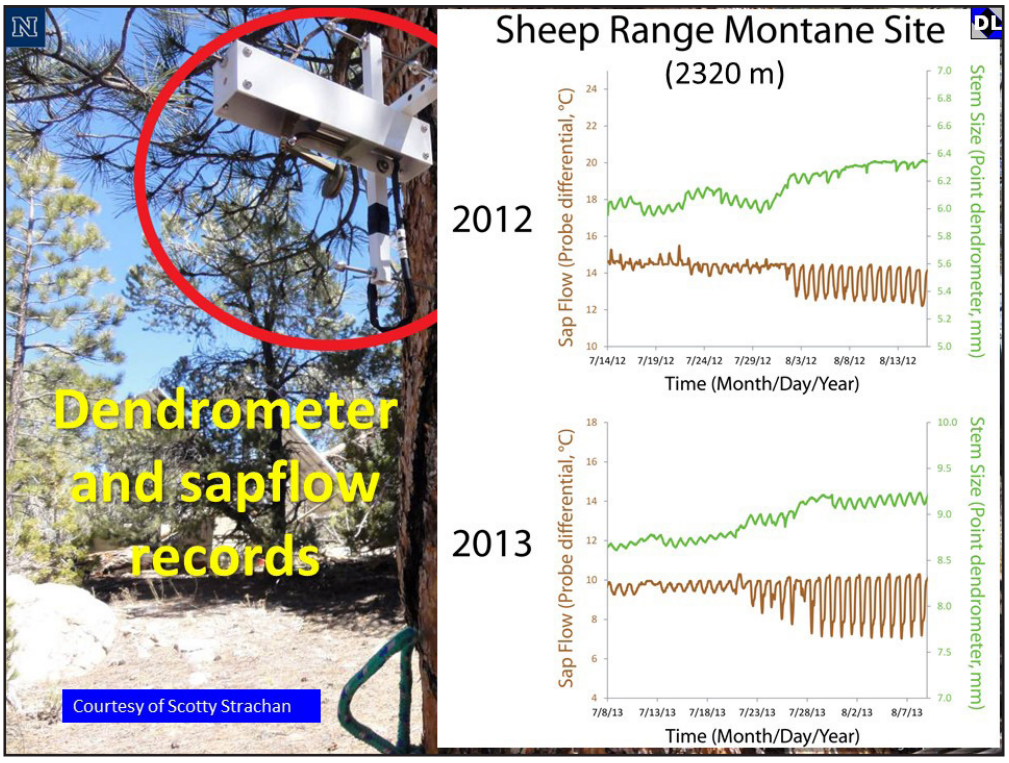

Figure 39. Dendrometer and sapflow records.

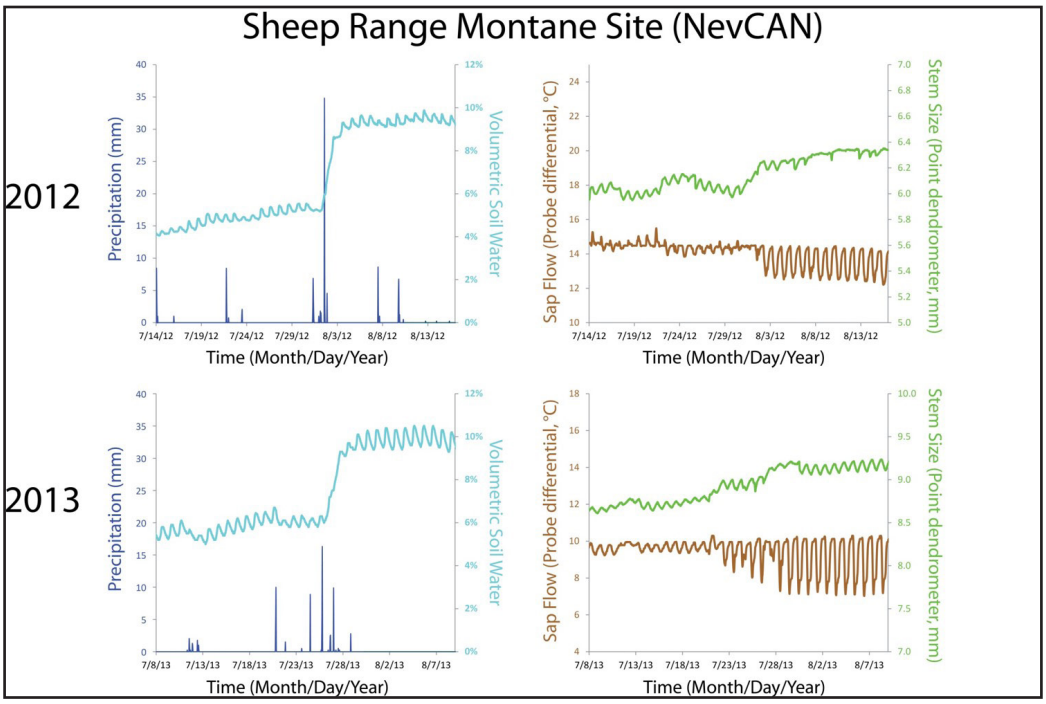

Figure 40. Climate sensitivity at sub-daily time scales.

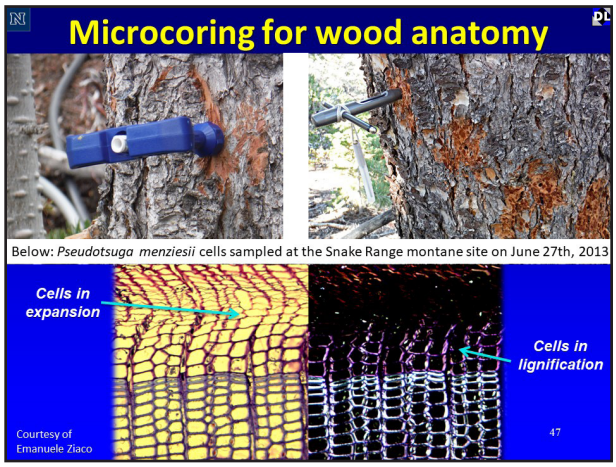

Figure 41. Microcoring for wood anatomy. Top left image shows microcoring with a surgical needle. Top right image shows microcoring with Trephor. The sampling spiral adopted to minimize damage and distortion when using the Trephor is visible in the top right image and has been adopted only on trees not equipped with dendrometers or sapflow sensors. Cellular structure (below). Staining with cresyl-violet was used to recognize cellular phases. Under normal illumination the thin-walled cells of the cambial zone (Cz) are clearly visible. Under polarized light the cambial zone and radially enlarging cells appear as a dark stripe (Cc), while cells in lignification (Lc; purple) can be easily distinguished from mature cells (Mc; blue) of the previous year. At the date of sampling, no mature cells had yet formed for the current growing season.

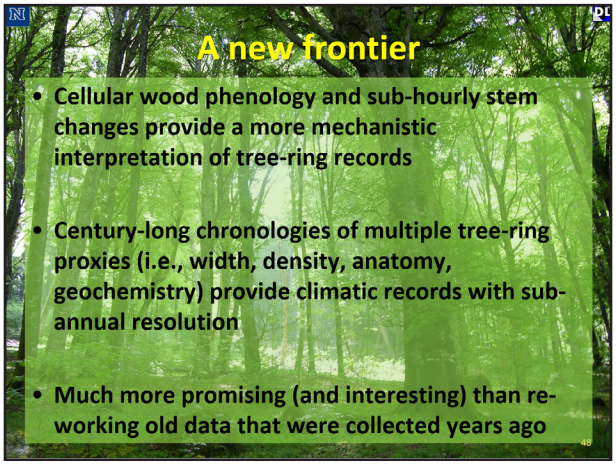

Figure 42. A new frontier.